

# **10x10 SVEA Fuel Critical Power Experiments and CPR Correlations:**

## **SVEA-96**

LEGAL NOTICE

THIS REPORT WAS PREPARED AS AN ACCOUNT OF WORK SPONSORED BY ABB COMBUSTION ENGINEERING NUCLEAR POWER, INC. NEITHER ABB COMBUSTION ENGINEERING NUCLEAR POWER, INC. NOR ANY PERSON ACTING ON ITS BEHALF:

A. MAKES ANY WARRANTY OR REPRESENTATION, EXPRESS OR IMPLIED INCLUDING THE WARRANTIES OF FITNESS FOR A PARTICULAR PURPOSE OR MERCHANTABILITY, WITH RESPECT TO THE ACCURACY, COMPLETENESS, OR USEFULNESS OF THE INFORMATION CONTAINED IN THIS REPORT, OR THAT THE USE OF ANY INFORMATION, APPARATUS, METHOD, OR PROCESS DISCLOSED IN THIS REPORT MAY NOT INFRINGE PRIVATELY OWNED RIGHTS; OR

B. ASSUMES ANY LIABILITIES WITH RESPECT TO THE USE OF, OR FOR DAMAGES RESULTING FROM THE USE OF, ANY INFORMATION, APPARATUS, METHOD OR PROCESS DISCLOSED IN THIS REPORT.

**CENPD-392-NP**

**10x10 SVEA Fuel Critical Power Experiments and CPR  
Correlations:**

**SVEA-96**

**December 1999**

**ABB Combustion Engineering Nuclear Power, Inc.**

Copyright 1999, ABB Combustion Engineering Nuclear Power, Inc.  
All Rights Reserved



## ABSTRACT

ABB is currently completing a program expanding the critical power data bases and developing improved Critical Power Ratio (CPR) correlations for ABB 10x10 SVEA fuel. Critical power data have been obtained for the SVEA-96, SVEA-96+ and SVEA-96 Optima designs. The SVEA-96 Optima design is an advanced product that has not yet been introduced in reload quantities. Based on measurements for these fuel designs, advanced CPR correlations utilizing the same general form have been established for the SVEA-96, SVEA-96+ and SVEA-96 Optima designs.

This report describes the development of the advanced critical power correlation for ABB SVEA-96 BWR fuel assemblies. The advanced CPR correlation for SVEA-96 fuel is referred to as ABBD1.0. A report (CENPD-389-P-A) that describes the corresponding advanced CPR correlation for SVEA-96+ fuel has been reviewed and accepted by NRC. It is anticipated that a subsequent report will be submitted for the SVEA-96 Optima design.

The current CPR correlation for the SVEA-96 assembly is referred to as the XL-S96 CPR correlation. The XL-S96 CPR correlation has been reviewed and approved by the NRC and is described in UR 89-210-P-A.

Three different test series have been performed for the ABBD1.0 CPR correlation development. These test series were performed with 24-rod sub-bundles with three different axial power shapes. The tests include measurements of critical power at pressures between [Proprietary Information Deleted] and an inlet subcooling temperature range from [Proprietary Information Deleted]. The mass flux range in the tests is [Proprietary Information Deleted]. The critical power measurements were performed at [Proprietary Information Deleted] different local power distributions to capture the influence on critical power of various local peaking factors and various peak power rod locations.

The SVEA-96 data from the measurements were correlated by adapting a critical power correlation with a critical quality/boiling length form [Proprietary Information Deleted]. This CPR correlation is referred to as the ABBD1.0 correlation.

The ABBD1.0 correlation predicts the measured critical powers over the entire data base with a mean error of [Proprietary Information Deleted].

<b>1. INTRODUCTION</b>	<b>1</b>
<b>2. TEST FACILITY</b>	<b>3</b>
2.1 Description	3
2.2 Test Section	3
2.3 Heater Rods	4
2.4 Power Supply and Control	5
2.5 Instrumentation	5
2.6 Data Acquisition System	6
2.7 Critical Power Testing Procedure	7
<b>3. TEST PROGRAM</b>	<b>14</b>
3.1 Range of Test Parameters	14
3.2 Justification for Range of Test Parameters	14
3.2.1 Mass Flux	15
3.2.2 System Pressure	15
3.2.3 Inlet Subcooling	15
3.2.4 Axial Power Distribution	15
3.2.5 Local Power Distribution	15
3.2.6 Combinations of Parameters	16
3.2.7 Summary	16
3.3 Data Validation Criteria and Procedures	16
3.4 Data Trends	17
3.4.1 SVEA-96 Sub-bundle Cosine Axial Power Shape Tests (SF24A)	18
3.4.2 SVEA-96 Sub-bundle Bottom-and Top-peaked Axial Power Shape Tests	18
<b>4. CRITICAL POWER CORRELATION</b>	<b>26</b>
4.1 Form of the Correlation	26
4.2 ABBD1.0 CPR Correlation	26
4.3 Calculation of the Sub-bundle R-factor for SVEA-96	27
4.4 Determination of ABBD1.0 Additive Constants and Correlation Coefficients	27
4.5 Assembly R-Factor - Treatment of Sub-bundle Power Mismatch	27
<b>5. CORRELATION EVALUATION</b>	<b>30</b>

5.1	ABBD1.0 Performance Relative to the SVEA-96 Data Base	30
5.2	Correlation Uncertainty and Range of the Correlation	32
6.	<b>CONFIRMATION FOR TRANSIENT APPLICATION</b>	<b>35</b>
6.1	Introduction	35
6.2	Transient Implementation Validation Methodology	36
6.3	Transient Dryout Experiments	36
6.3.1	FRIGG Loop	36
6.3.2	Test Section	36
6.3.3	Transient Tests Description	37
6.3.4	Dryout Threshold Temperature	37
6.3.5	Transient Data	37
6.4	Implementation Validation for BISON Code	37
6.4.1	BISON Code	38
6.4.2	BISON Model	38
6.4.3	BISON Test Simulation Results	38
6.5	Summary	39
7.	<b>CONCLUSIONS</b>	<b>42</b>
8.	<b>REFERENCES</b>	<b>43</b>
APPENDIX A	<b>SVEA-96 ASSEMBLY DESCRIPTION</b>	<b>A-1</b>
APPENDIX B	<b>SVEA 96 STEADY STATE CRITICAL POWER TEST DATA (BOTTOM-PEAKED AXIAL POWER SHAPE)</b>	<b>B-1</b>
APPENDIX C	<b>SVEA 96 STEADY STATE CRITICAL POWER TEST DATA (TOP-PEAKED AXIAL POWER SHAPE)</b>	<b>C-1</b>

## 1. INTRODUCTION

This report describes the development of an advanced critical power ratio (CPR) correlation for the ABB SVEA-96 water cross BWR fuel assembly. The SVEA-96 fuel assembly is described in detail in UR-89-210-P-A (Reference 1). The SVEA-96 assembly is composed of four sub-bundles in a 5x5 lattice configuration with one fuel rod missing and [Proprietary Information Deleted] For convenience, a brief overview of the SVEA-96 assembly is provided in Appendix A.

The current CPR correlation for the SVEA-96 assembly is referred to as the XL-S96 CPR correlation. The XL-S96 CPR correlation has been reviewed and accepted by the NRC and is described in Reference 1. The XL-S96 CPR correlation was developed based on cosine axial power shape tests. The CPR correlation for SVEA-96 fuel described in this report is based on an expanded data base including top-peaked and bottom-peaked axial power shape data and is referred to as ABBD1.0. The SVEA-96+ testing and correlation development program discussed in References 5 through 7 indicated a SVEA-96 assembly CPR correlation based on an expanded data base including top-peaked and bottom-peaked axial power shape data in conjunction with the form used for ABBD2.0 could represent an improvement relative to the XL-S96 correlation described in Reference 1.

The SVEA-96 Critical Power data obtained for a cosine axial power shape is described in Section 3 and Appendix A of Reference 1. These data have also been used in the development of the ABBD1.0 CPR correlation described in this report. The ABBD1.0 CPR correlation data base also contains Critical Power measurements based on top-peaked and bottom-peaked axial power shapes. The Critical Power measurement data based on top-peaked and bottom-peaked axial power shapes are contained in this report. The sub-bundle R-factor model in the XL-S96 CPR correlation has been retained for the ABBD1.0 correlation. As shown in this report, the additive constants developed for the XL-S96 CPR correlation in Reference 1, in conjunction with the optimized ABBD1.0 correlation parameters, provide a good fit to the expanded SVEA-96 data base containing cosine, top-peaked, and bottom-peaked axial power shapes. Therefore, the additive constants developed in Reference 1 were retained for the ABBD1.0 CPR correlation, and the description of their derivation is not repeated in this report. The practice of basing the derivation of additive constants on the cosine axial power shape data base was also successfully applied to the ABBD2.0 CPR correlation described in References 5 through 7.

The critical power test section consisted of a 24-rod bundle simulating a sub-bundle of the SVEA-96 fuel assembly. Indirectly heated rods connected to several individual rectifier units made it possible to control the local power (i.e. relative rod power) distribution in a simple way and test a wide range of local power distributions. The objectives of these tests and the CPR evaluation program were as follows:

1. To expand the SVEA-96 data base to include top-peaked and bottom-peaked axial power shapes and to support the same type of CPR correlation formulation which has been adopted for SVEA-96+ fuel (Reference 5).

2. To confirm that the CPR correlation for the SVEA-96 assembly (ABBD1.0) developed from the steady state critical power data base adequately describes the data base and to establish appropriate biases and uncertainties for licensing applications. Since the correlation was developed from steady state data, it will provide best estimate CPR values for steady state applications. For licensing applications, the correlation will be applied in computer codes accepted by the NRC.
3. To confirm that the CPR correlation for the SVEA-96 assembly (ABBD1.0) established under steady state conditions provides an adequate description of the change in critical power ( $\Delta$ CPR) during transient applications. This confirmation is performed by comparing the predictions of the ABBD1.0 CPR correlation for transient conditions with available transient CPR test data. The ABBD1.0 CPR correlation is compared with the same SVEA-96 transient data base described in Reference 1. The ABB methodology for performing this confirmation is illustrated for the BISON-SLAVE code documented in Reference 2.

The test matrix described in Reference 1 and in this document was selected to cover the entire steady state and transient operating range expected for U.S. BWR's and to sufficiently cover off nominal conditions to allow its application to transient and accident conditions. Particular emphasis has been placed on capturing the dependence of local power distributions within the bundle since this is expected to be a very important bundle-specific effect.

The ABBD1.0 critical power correlation developed for the SVEA-96 assembly is a critical quality-boiling length form [Proprietary Information Deleted]. It is referred to as the ABBD1.0 correlation [Proprietary Information Deleted].

The degree to which the correlation fits the experimental data is reflected by the average percent deviation of the correlation prediction relative to the measured critical power over the entire data range. [Proprietary Information Deleted]. The ABBD1.0 CPR correlation has been implemented in the BISON-SLAVE dynamic system transient analysis code. Conservative predictions of CPR behavior during postulated transients has been demonstrated by comparisons of BISON-SLAVE code/ABBD1.0 correlation predictions with FRIGG Loop dynamic flow reduction test data. These results using ABBD1.0 provide further confirmation of the conclusion reached in Reference 5 that a CPR correlation with the ABBD1.0/ABBD2.0 correlation form derived from steady-state data in conjunction with the BISON-SLAVE code provides a conservative treatment of CPR changes during postulated transients. The evaluation in Section 6 provides an illustration using the BISON-SLAVE dynamic code of the ABB methodology for confirming that a CPR correlation based on steady-state data conservatively predicts CPR behavior under transient conditions. This methodology can also be used to confirm that other CPR changes during transient events are conservatively treated in other dynamic codes.

## 2. TEST FACILITY

The cosine axial power shape tests supporting the ABBD1.0 CPR correlation were described in detail in Reference 1. The additional test results with bottom-peaked and top-peaked axial power shapes supporting the ABBD1.0 CPR correlation are described in this document.

All of the cosine, top-peaked, and bottom-peaked axial power shape data supporting the ABBD1.0 CPR correlation were performed in the FRIGG Loop test facility. This facility, as well as the measurement of the cosine shaped axial power shape data, were described in Reference 1. Therefore, the description of the test facility and measurements in this document is focused on the measurement of the top- and bottom-peaked axial power shaped data.

### 2.1 Description

The SVEA-96 critical power tests were performed in the FRIGG loop at the ABB Atom laboratories at Vasteras, Sweden. The FRIGG loop has been utilized for many years to perform thermal hydraulic tests in support of the ABB BWR nuclear program.

A diagram of the FRIGG loop is shown in Figure 2.1. The loop contains a main circulation loop with the test section, a cooling circuit, and a purification system. The head of the main circulation pump can be continuously controlled by means of a variable speed motor. When steam is produced in the test section, the loop pressure is controlled by regulating the cold water flow to spray nozzles in the condenser. Heat is removed by a heat exchanger in the cooling circuit from which water is pumped to the spray nozzles. During start-up and heat balance tests, the loop is filled with water, and the pressure is regulated by balancing the amount of water by means of the feed water pump and a drainage valve. The inlet subcooling is controlled by feeding water from the cooling circuit into the main circulation loop upstream of the pump.

The loop is designed for a maximum pressure of 100 bar and a maximum temperature of 311 °C. Carbon steel is used throughout as a construction material, and water quality is carefully controlled. Demineralized and deaerated water is used for filling the loop. Purification is continued during the tests to keep water quality within specified limits. Normally water conductivity is in the range of 0.15 - 0.30  $\mu\text{S}/\text{cm}$ .

### 2.2 Test Section

The test section consists of a pressure vessel, a Zircaloy flow channel and a SVEA 5x5-1 sub-bundle with 24 heater rods. [Proprietary Information Deleted]. To avoid deformation at extreme test conditions and the subsequent flow redistribution, the flow channel is reinforced by an outer support structure. Pressure taps are connected to the flow channel at different elevations as shown in Figure 2.2. The pressure transmission lines are brought out of the test section through an instrumentation ring.

An orifice plate is installed at the inlet of the flow channel to provide an even distribution of flow into the channel. **[Proprietary Information Deleted]**.

The heated rods are constrained by six Inconel spacers of the same type used in the standard reload SVEA-96 assembly. Additional Inconel spacers which are not used in the standard SVEA-96 are positioned at the inlet and exit of the test section. These additional spacers do not impact the dryout results. The axial locations of the spacers and the pressure taps (DP) are shown in Figure 2.2.

The pressure vessel top flange contains pressure seals similar in design to valve stem packing seals, which retain the heater rods in fixed position. The difference in thermal expansion between the heater rods and the pressure vessel is taken care via O-ring pressure seals in the bottom flange.

Dimensions of the test section are compared with actual SVEA-96 design parameters in Figure 2.3. The design dimensions of the SVEA-96 test section, which might affect dryout, are not identical to those of the standard SVEA-96 reload fuel assembly. **[Proprietary Information Deleted]**. Therefore, the effects on critical power of the small differences between the SVEA-96 sub-bundle test section geometry and the reload fuel assembly are either negligible or are accounted for in the correlation. It should be noted that minor differences in the flow area of the test sections used for the three axial power shape test series due to the slight variations in the diameter of the rods were specifically accounted for in the correlation derivation and evaluation.

The numbers assigned to the heater rods in Figure 2.3 are used to identify the heater rods in Appendices B and C. As shown in Figure 2.3, the heater rod numbering scheme identifies the rod location in the sub-bundle.

Tables 2.1 through 2.3 and Figure 2.4 show the axial power shapes used in the three 24-rod sub-bundle test series.

### 2.3 Heater Rods

The heater rods used in the tests are indirectly heated rods rated at 200 kW at 380 V DC. A heater rod schematic is shown in Figure 2.5. Each heater rod contains a heater element, electrical insulation, Inconel-600 cladding, and **[Proprietary Information Deleted]**. The heater element is made from a Monel K-500 tube. The heater element terminals consisted of a solid nickel transition piece welded to the Monel tube at one end, and a copper electrode brazed to the Monel tube at the other end. The heater-rod non-uniform axial power profile was generated by laser cutting a spiral on the Monel tube with a variable pitch.

The electrical insulation was machined from solid boron nitride (BN) pieces. After the BN sleeves were assembled over the heater element, grooves were cut axially to hold the thermocouples in position. Then the heater element assembly was inserted into the oversized Inconel tube used as cladding. The final heater rod dimensions were obtained by swaging the heater assembly to its final dimensions. The swaging operation also provided good contact between the heater element, the insulation material, and the cladding inner surface assuring good heat transfer with low variability from the heating element to the cladding surface.

The thermocouples (dryout detectors) are embedded between the cladding and the insulation sleeves. The thermocouples used were 0.5 mm ungrounded Inconel sheathed type K with MgO insulation. The thermocouple wire used was of premium grade. The thermocouple tips were backfilled with BN powder and compacted by swaging to provide a faster response to temperature changes.

**[Proprietary Information Deleted].** Figure 2.6 shows the rod types and the axial positions of the thermocouples used in the bottom-peaked axial power shape tests. Figure 2.7 shows the rod types and the axial positions of the thermocouples used in the top-peaked axial power shape tests.

It should be noted that in Figures 2.6 and 2.7, rod types "A" and "B" are identical with the exception of the thermocouple locations. As shown in Figure 2.6, fifteen B-type and nine A-type rods were used in the bottom-peaked axial sub-bundle tests. The thermocouples in the B-type rods in this test series are located in positions to assure that dryout with a bottom-peaked axial power shape will be detected. The thermocouples in the A-type rods are not positioned in a manner to indicate dryout. Therefore, A-type rods are placed only in symmetrical positions to the B-type rods in the bottom-peaked test section. The relative powers for the A-type rods were maintained sufficiently lower than the B-type rods in the bottom-peaked sub-bundle tests to assure that dryout would not occur on the A-type rods. As shown in Figure 2.7, fifteen A-type and nine B-type rods were used in the top-peaked axial sub-bundle tests. The thermocouples in the A-type rods in this test series are located in positions to assure that dryout with a top-peaked axial power shape will be detected. The thermocouples in the B-type rods are not positioned in a manner to indicate dryout. Therefore, B-type rods are placed only in symmetrical positions to the A-type rods in the top-peaked test section. The relative powers for the B-type rods were maintained sufficiently lower than the A-type rods in the top-peaked sub-bundle tests to assure that dryout would not occur on the B-type rods.

## 2.4 Power Supply and Control

For the top-peaked and bottom-peaked axial power shape tests, electrical power to the heater rods was supplied by a 4.5 MW DC electrical power system operating at 380 V. The system consisted of seven units, all rated at 640 kW each.

The upgraded FRIGG loop has a very flexible system for connecting the individual heater rods to selected units. This configuration provides the capability to conveniently obtain numerous combinations of relative rod powers by adjusting the computer signals that control the voltage across each unit. It is this capability which allows a thorough determination of sub-channel factors (e.g. R-factors) providing the relative dryout sensitivity of each fuel rod.

## 2.5 Instrumentation

The parameters defining the operating conditions during the tests consist of temperature, pressure, flow, differential pressure and bundle power. These variables and the method by which they are monitored are defined as follows:

p (bar) is the pressure at the test section outlet. The pressure is measured with a precision pressure transducer in the test section inlet. Estimated accuracy in the measured pressure is  $\pm 0.5$  bar.

$\Delta T$  sub ( $^{\circ}\text{C}$ ) is the inlet subcooling. This parameter is defined as the difference between the saturation temperature at the test section outlet and the test section inlet temperature. The temperatures were measured with type-K premium grade thermocouples for the SVEA-96 sub-bundle tests. Estimated accuracy in the measured inlet subcooling is  $\pm 1$   $^{\circ}\text{C}$ .

Q (kW) is the power provided to the coolant by the rod bundle. The power is obtained by the summation of the power generated by each heater rod. Heater rod power is calculated as the product of measured current through each rod multiplied by the measured voltage drop across the rod group in which the heater rods are connected. Heater rod current is measured by a calibrated precision shunt connected to the ground electrical leads.

The bundle power is obtained by reducing the measured power by 0.4% to account for the heat generated in heater rod extensions at the inlet and outlet. This power is dissipated in the flanges and is not delivered to the coolant. The estimated accuracy in measured bundle power is  $\pm 1\%$  of the reading at power levels typical at dryout.

$G = \dot{m} / A$  ( $\text{kg}/\text{m}^2\text{s}$ )

is the mass flux. A is the flow area in the test bundle at room temperature. The flow rate,  $\dot{m}$ , is measured with an orifice plate in the recirculation line. The estimated accuracy in G is 20  $\text{kg}/\text{m}^2\text{s}$ .

The above accuracies in the major variables represent an accuracy (tolerance) in critical power of about  $\pm 2\%$ .

Rosemount differential pressure (D/P) cells, calibrated to an accuracy of  $\pm 0.5\%$  of full scale, were used to measure pressure drops across various part of the bundle and across the main line flow meter. The main line flow meter was equipped with two D/P cells having different ranges in order to minimize the flow measurement error due to errors in differential pressure measurements.

Thermocouples were located at five elevations along the test vessel in order to measure the fluid temperature in the annulus between the pressure vessel and the flow channel (i.e. the temperature in the bundle differential pressure transmission lines).

## 2.6 Data Acquisition System

A typical data acquisition system is shown in Figure 2.8. Signals reflecting important parameters (e.g. temperature, voltage, current differential pressure and

mass flow) are connected to HP3852A data loggers. A sampling frequency of 1.0 Hz was used.

In addition to the data collecting function, the computer was also used as a dryout monitor by utilizing software which allows it to recognize a temperature rise over the initial local temperature in up to 112 heater rod thermocouples. In this case the computer identified the channel(s) indicating dryout. Steady state dryout is assumed to occur for a minimum measured temperature rise of **[Proprietary Information Deleted]**.

In addition to the dryout indication, two additional limits were used to protect the bundle. A temperature rise of 50 °C and a temperature above 450 °C automatically cause a decrease in bundle power of 25%. A temperature rise of 75 °C causes the bundle power to be shut off completely.

The dryout monitoring function must be in operation before power is provided to the test section. When dryout was detected, the loop conditions were kept constant for about 20 seconds to clearly define average loop conditions at dryout for that test point.

## 2.7 Critical Power Testing Procedure

The measuring instruments used and the data acquisition system are discussed in Sections 2.5 and 2.6. The tests were recorded in blocks of a maximum size of 2400 samples of each parameter, which corresponds to 2400 seconds at a sampling frequency of 1 Hz. Each block generally included several critical power measurements at different mass flows.

The procedure for establishing critical power was as follows:

- The test identification number was entered into the computer.
- The target local power distribution was entered into the computer, which established the corresponding rectifier settings.
- The target bundle inlet subcooling temperature, system pressure, and mass flux were established.
- The bundle power was slowly increased in small steps. The power was increased until a temperature excursion exceeding **[Proprietary Information Deleted]** occurred and triggered an alarm. All the thermocouples were connected to the data loggers, and their outputs recorded during the test. In addition, selected thermocouple outputs were displayed on a monitor in the control room.

**TABLES 2.1 THROUGH 2.3**  
**[PROPRIETARY INFORMATION DELETED]**

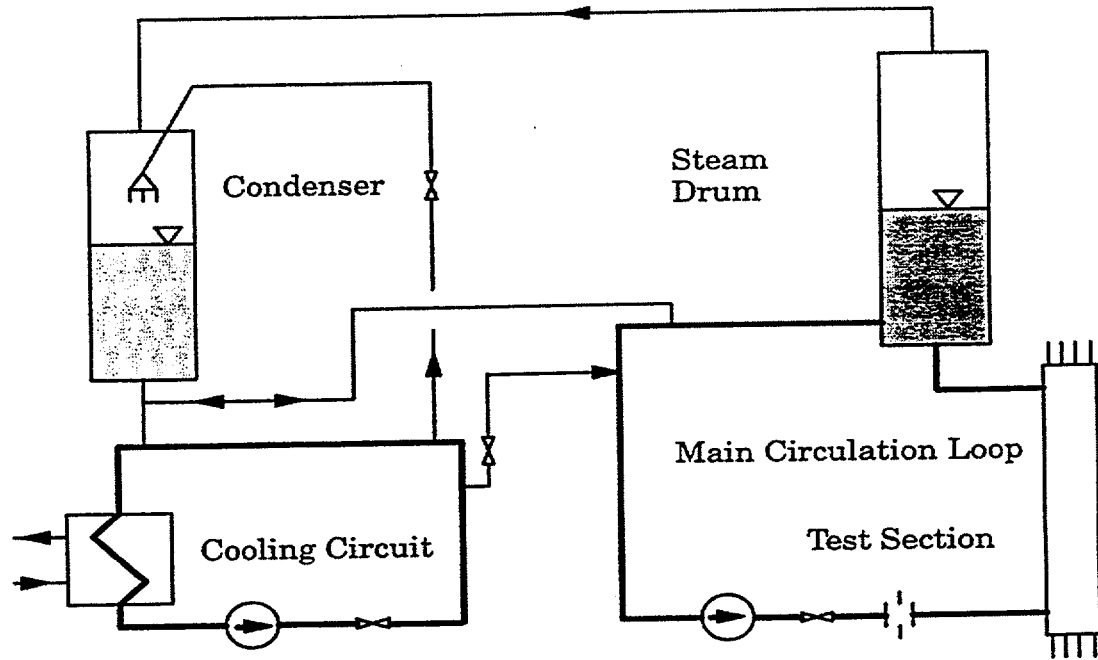


Figure 2.1 FRIGG loop diagram

**FIGURES 2.2 THROUGH 2.4**  
**[PROPRIETARY INFORMATION DELETED]**

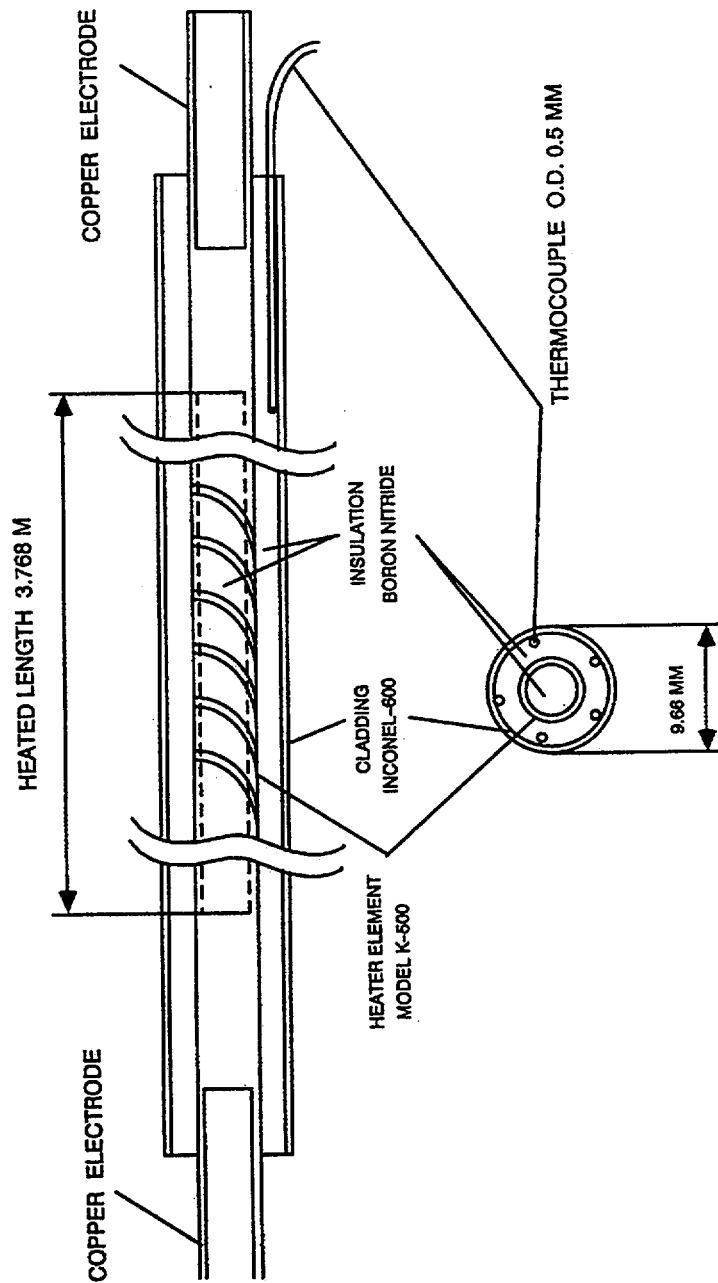


Figure 2.5 Heater rod design

**FIGURES 2.6 THROUGH 2.7**  
**[PROPRIETARY INFORMATION DELETED]**

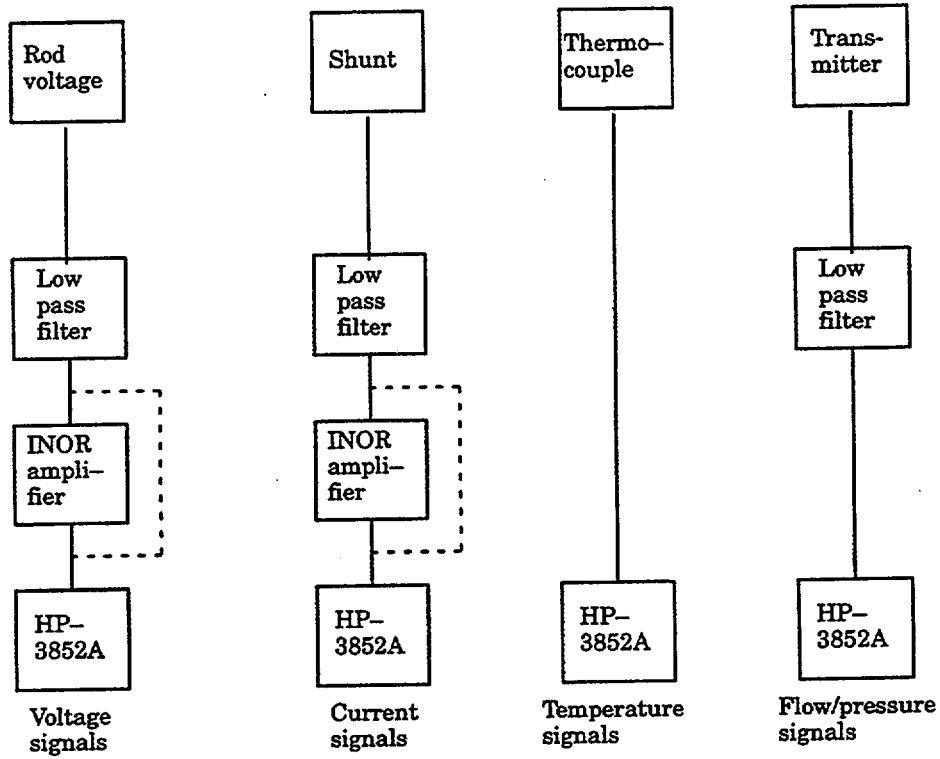


Figure 2.8 Data acquisition system

### 3. TEST PROGRAM

As discussed in Section 2, the test program included three separate test series. These series were performed with full-length SVEA-96 24-rod sub-bundle test sections. The three sub-bundle test series differ with respect to the axial power shape provided by the heater rods. Sub-bundle data were obtained for cosine, bottom-peaked, and top-peaked axial power shapes. The test results for the three sub-bundle test series are given in Appendix A of Reference 1 (cosine axial power shape), Appendix B of this document (bottom-peaked axial power shape), and Appendix C of this document (top-peaked axial power shape). The test series are identified by the following test identification ranges:

<b>Axial Power Shape</b>	<b>Initial Test Point</b>	<b>Final Test Point</b>	<b>Data Point Table</b>
Cosine	1104-1-AA	2118-10-KLL	Ref. 1, Appendix A
Bottom-Peaked	1033-1-AA4	1091-48-AA16	Appendix B
Top-Peaked	1025-1-AA4	1090-16-AA13	Appendix C

The number of data points and local power distributions in the cosine, bottom-peaked, and top-peaked test series are summarized in Table 3.1. As noted in Reference 1 and Appendices B and C of this document, the actual local power distribution at which the data point was measured may differ slightly from the nominal distribution. The local power distributions actually measured for each data point, and the R-factor corresponding to that distribution, were used in the correlation derivation and evaluation.

#### 3.1 Range of Test Parameters

The ranges of test parameters over which the sub-bundle critical power tests were conducted are shown in Table 3.2.

Histograms defining the ranges of mass flux, pressure, inlet subcooling, and local power distribution as reflected by the CPR correlation R-factor values are shown in Figures 3.1a through 3.1d, 3.2a through 3.2d, 3.3a through 3.3d, and 3.4a through 3.4d, respectively. In each case, the figure denoted "a" is a histogram showing the entire range of data for all three axial power shapes. The figures denoted "b", "c", and "d" indicate histograms showing the range of data for the cosine, bottom-peaked, and top-peaked axial power shapes, respectively. The number of data points obtained in each parameter range (mass flux, pressure, inlet subcooling) are also shown in Tables 3-3 through 3-6 for the cosine axial power shape tests, bottom-peaked axial power shape tests, and top-peaked axial power shape tests, respectively.

[Proprietary Information Deleted].

#### 3.2 Justification for Range of Test Parameters

The critical power performance of a test bundle is a function of mass flux, system pressure, inlet subcooling, axial power distribution, and local power distribution. The range of the test parameters for which the critical power tests were conducted is presented in Section 3.1. Justification for the ranges is summarized in the following subsections.

### 3.2.1 Mass Flux

The critical power is a strong function of mass flux. Therefore, data were obtained at numerous points [Proprietary Information Deleted] over the range of mass flux considered to establish the correlation at various values of pressure, inlet subcooling, and bundle local powers.

[Proprietary Information Deleted]. The range of mass flux representing normal operations and AOOs is very broad [Proprietary Information Deleted]. The mass flux points used for the tests cover this expected operating range.

### 3.2.2 System Pressure

Data were obtained at 6 different system pressures: [Proprietary Information Deleted]. This range provided sufficient data to determine the system pressure dependence of critical power over the expected range of application of the correlation. [Proprietary Information Deleted].

### 3.2.3 Inlet Subcooling

It is well known (e.g. References 1, 3 and 5) that critical power is a linear function of the inlet subcooling at constant mass flux and system pressure. [Proprietary Information Deleted] A 10 °C inlet subcooling corresponds to the reactor normal operating condition, and 45 °C inlet subcooling covers the loss of feedwater heating Anticipated Operational Occurrence.

### 3.2.4 Axial Power Distribution

Sub-bundle critical power data were obtained for a chopped cosine axial power distribution as well as for bottom-peaked and top-peaked axial power shapes. The cosine axial power shape is reasonably representative of typical operation. The bottom-peaked and top-peaked axial power shapes were selected to capture the effect of axial power shape over the range expected in reactor operation.

### 3.2.5 Local Power Distribution

The critical power performance of a test bundle is dependent on the test bundle local power distribution. One advantage of the FRIGG test loop is that the test bundle local power distribution can be easily varied. Systematic series of tests were conducted to investigate the critical power performance at various local peaking factors and various peak power rod locations. SVEA-96 critical power measurements were obtained at [Proprietary Information Deleted] to establish the effect of local power distribution on critical power. Figure 3.1 in Reference 1 and Appendices B and C of this document show the nominal local power distributions tested. The local power distribution may differ slightly from point-to-point in tests with the same nominal radial power distribution. The local power distribution actually measured for each data point was used in the correlation development and evaluation.

The local power distributions used in the tests were designed to establish the local power distribution dependence of the bundle critical power performance. The local power distributions involve rods with peaking factors between [Proprietary Information Deleted].

To summarize the discussion of the range of individual parameters in Sections 3.2.1 through 3.2.5: the ranges of parameters shown in Figures 3.1 through 3.4 were selected to cover values of parameters impacting Critical Power expected during normal BWR operations as well as Anticipated Operational Occurrences (AOOs) and accidents. In selecting the test matrices, greatest emphasis is placed on those regions in which the reactor will usually operate. Therefore, while pressure and inlet subcooling ranges of [Proprietary Information Deleted]. The mass flux points shown in Figures 3.1a through 3.1d cover this range. The range of local power distributions were selected to cover local power distributions expected during reactor operations and to allow an accurate determination of the dryout sensitivity of each rod in the sub-bundle. [Proprietary Information Deleted].

### 3.2.6 Combinations of Parameters

In order to confirm that the parameter ranges considered in the Critical Power tests cover the combinations of conditions expected during typical reactor application, the parameter ranges expected during reactor application (See Table 3.7) are superimposed on the ranges of test points for various combinations of test parameters in Figures 3.5 through 3.10. The expected boundaries of typical reactor application are shown by rectangles in these figures. As shown in Figures 3.5 through 3.10, the ranges of parameters including combinations of parameters at their extremities (i.e. "corner to corner" ranges) expected during typical reactor operation are adequately covered by the ranges of test points. Figures 3.5 through 3.7 confirm that the ranges of mass flux, inlet subcooling, and pressure expected during reactor operation are within the corresponding ranges considered in the tests. Figures 3.8 through 3.10 indicates that the expected sub-bundle R-factor range for potentially limiting assemblies during reactor operation is sufficiently well represented by the sub-bundle data base.

### 3.2.7 Summary

A side by side comparison of the range of the parameters in the tests with that of a typical reactor application is shown in Table 3.7. The combined range is based on the composite range of all the tests and is considered to be the range of validity of ABBD1.0. As discussed in Section 3.2.6 and seen in Table 3.7, the range for a typical application is adequately bounded by the range of validity of ABBD1.0.

[Proprietary Information Deleted].

### 3.3 Data Validation Criteria and Procedures

Data validation is supported with instrumentation performance reliability checks. All data collection instrumentation is periodically calibrated to assure the accuracy of the data.

The data validation process is further reinforced by assuring that all instrumentation is checked for proper operation prior to the performance of each test. Before and after each shift, a reading from every transmitter is recorded and compared with the expected value for that transmitter. In the event of an abnormal reading, corrective actions are taken before the actual test is run. In addition, the following checks are performed at the beginning of each test period:

1. A heat balance is calculated to insure that power, flow, and temperature measurements are correct.
2. The overall pressure drops across the bundle at different flow rates are measured.
3. The sum of the power generated by each heater rod is compared with the sum of the power outputs from each power supply unit for all test points. These two bundle power measurements are accepted if they agree to within  $\pm 1\%$ .

Critical power reference test points are periodically repeated to assure that the measurements are stable. The reference points for the SVEA-96 test series are defined by the following nominal conditions:

Bundle Outlet Pressure	[Proprietary Information Deleted].
Inlet Subcooling	[Proprietary Information Deleted].
and with mass flux covers the range	[Proprietary Information Deleted].

These reference test measurements were performed, at a minimum, for a uniform local power distribution.

The reproducibility of the critical power was found to be very good for the SVEA-96 test series. Examples of the reproducibility are shown in Table 3.8.

Conversion of the data to engineering units by the computer allowed preliminary test validation to be done upon completion of a run and before the data analysis took place. This preliminary validation provided immediate feedback on facility operation and data collecting equipment performance.

After the instrumentation had been functionally checked, and the test parameters and performance had been compared with the test matrix, the final data validation was performed during the data reduction and analysis stage.

### 3.4 Data Trends

This section shows trends in the measured Critical Power data. These trends are addressed to confirm that the SVEA-96 Critical Power database is physically realistic and consistent with similar measurements obtained for other assembly designs. The figures in this section show the measured data points and the corresponding ABBD1.0 Correlation predictions (See Section 4) of the data measurements. The correlation predicted critical power data is denoted with suffix "Pred". Furthermore, it should be noted that some spurious spread is introduced

into the data when it is plotted in this manner since all of the points were not obtained at precisely the target condition.

A test bundle is referred to with a designation such as SF24A. The designation SF24A (S=SVEA, F=FRIGG, 24 = number of rods, A = a serial number) stands for dryout power measurements on a SVEA-96 sub-bundle test section with the cosine axial power shape. The designation SF24AB refers to dryout power measurements on a SVEA-96 sub-bundle test section with the bottom-peaked axial power shape. The designation SF24AT refers to dryout power measurements on a SVEA-96 sub-bundle test section with the top-peaked axial power shape.

#### 3.4.1 SVEA-96 Sub-bundle Cosine Axial Power Shape Tests (SF24A)

The SVEA-96 data trends for the cosine axial power shape obtained with the SF24A test section were presented in Section 4 of Reference 1 and are not repeated in this document. The evaluation of the SVEA-96 Critical Power data based on a cosine axial power shape in Section 4 of Reference 1 showed that the dependence of the SVEA-96 test data on hydraulic parameters agrees with the critical power data taken for other designs and at other facilities.

#### 3.4.2 SVEA-96 Sub-bundle Bottom-and Top-peaked Axial Power Shape Tests

The results from the bottom-peaked (SF24AB) and top-peaked (SF24AT) tests at approximately **[Proprietary Information Deleted]** are compared with the results from the SF24A tests for these local power distributions (uniform, optimized, and realistic) in Figures 3.11, 3.12 and 3.13. "Uniform" local power distributions are intended to provide the same power to each of the 24 heater rods. The term "optimized" refers to a rod power distribution that gives the highest dryout power for a given set of mass flux, system pressure, inlet subcooling and axial power shape conditions. The optimized rod power distribution is achieved by **[Proprietary Information Deleted]**. A "realistic" local power distribution represents a typical power distribution expected during assembly operation.

The critical power decreases as the axial power shapes become more top-peaked in Figures 3.11 through 3.13. This tendency is in agreement with measurements obtained for other assembly designs such as the SVEA-96+ design discussed in Reference 5. The monotonic increase in Critical Power as a function of mass flux is also consistent with other designs and the data obtained in other facilities. Therefore, the trends in these data reflect the expected dependence on assembly flow and axial power shape based on previous testing of earlier designs and the physical nature of the dryout process for various local power distributions.

Trends in exit pressure and inlet subcooling for various local power distributions are shown for the bottom-peaked axial power distribution (test bundle SF24AB) and the top-peaked axial power distribution (test bundle SF24AB) in Figures 3.14 through 3.19 and Figures 3.20 through 3.24, respectively.

The influence of inlet subcooling at an **[Proprietary Information Deleted]**.

Critical power as a function of pressure for various constant mass flows and inlet subcoolings are shown in Figures 3.16 to 3.19 for the bottom-peaked axial power shape and Figures 3.22 to 3.24 for the top-peaked axial power shape. As shown in

these figures, **[Proprietary Information Deleted]** The same type of behavior as a function of system pressure was observed for the SVEA-96+ design reported in Reference 5 and is also consistent with other earlier designs.

The purpose in providing data trend plots in Figures 3.14 through 3.24 is to show that the trends in the data are physically reasonable and consistent with expectations. ABBD1.0 predictions are included in these figures to help the correlation review as previously requested in the review of the ABBD2.0 Correlation (Reference 5).

**TABLES 3.1 THROUGH 3.8**  
**[PROPRIETARY INFORMATION DELETED]**

**FIGURES 3.1a THROUGH 3.4a**  
**[PROPRIETARY INFORMATION DELETED]**

**FIGURES 3.1b THROUGH 3.4b**  
**[PROPRIETARY INFORMATION DELETED]**

**FIGURES 3.1c THROUGH 3.4c**  
**[PROPRIETARY INFORMATION DELETED]**

**FIGURES 3.1d THROUGH 3.4d**  
**[PROPRIETARY INFORMATION DELETED]**

**FIGURES 3.5 THROUGH 3.24**  
**[PROPRIETARY INFORMATION DELETED]**

## 4. CRITICAL POWER CORRELATION

### 4.1 Form of the Correlation

There are two common methods used to correlate critical power test data. One is to correlate the critical power test data in the critical quality-boiling length plane, and the other method is to correlate the critical power data in the critical heat flux-quality plane.

The critical quality-boiling length form has been selected to correlate the SVEA-96 critical power test data.

Since the trends in the SVEA-96 data are similar to trends for other BWR fuel, a critical quality-boiling length correlation would be expected to accurately correlate the SVEA-96 data.

This decision is confirmed by the results in Section 5 which demonstrate that a critical quality - boiling length correlation [**Proprietary Information Deleted**] sufficiently capture the dependence of all important parameters to which CPR is sensitive for the SVEA-96 design. This SVEA-96 critical power ratio correlation is described in this section and is referred to as ABBD1.0.

Experience has also shown that a critical quality-boiling length correlation represents a proven form capable of adequately predicting the onset of dryout during a transient. The process to confirm that ABBD1.0 provides an adequate prediction of the change in critical power during a transient code application is described in Section 6.

[**Proprietary Information Deleted**].

Finally, application of the ABBD1.0 correlation based on sub-bundle data to a full SVEA-96 assembly in a manner that assures critical powers will not be overpredicted requires a further modification to the R-factor. This modification accommodates sub-bundle power mismatch.

These adaptations to the critical quality-boiling length correlation form [**Proprietary Information Deleted**] resulted in the ABBD1.0 CPR correlation. The ABBD1.0 CPR correlation is described in this section.

### 4.2 ABBD1.0 CPR Correlation

Like the GEXL Correlation described in Reference 3, the ABBD1.0 and XL-S96 CPR correlations are both based on a critical quality-boiling length relationship. The form of the ABBD1.0 CPR Correlation is identical to that of the ABBD2.0 Correlation described in References 5 through 7 and, therefore, is not the same form as the XL-S96 Correlation described in Reference 1. The XL-S96 CPR correlation uses the critical quality given by the GEXL correlation and appropriate correction factors. ABBD1.0 and ABBD2.0 correlate critical quality to second order polynomials in mass flux, pressure, boiling length, R-factor and annular flow length and include all cross terms. A detailed description of the differences in form between the ABBD2.0 Correlation and XL-S96 is provided in the ABB response to NRC Request Number 2 in Reference 6. The description in the

response to Request Number 2 in Reference 6 also applies to the ABBD1.0 correlation.

All parameters discussed below are in SI units unless otherwise noted.

**[Proprietary Information Deleted].**

#### 4.3 Calculation of the Sub-bundle R-factor for SVEA-96

The R-factor accounts for the local power distribution, cross section geometry, and the spacer grid configuration.

**[Proprietary Information Deleted].**

#### 4.4 Determination of ABBD1.0 Additive Constants and Correlation Coefficients

As shown in Table 3.1, the SVEA-96 data base is extensive. Therefore, a systematic approach was required to establish the additive constants and correlation coefficients:

1. The SVEA-96 additive constants in Figure 4.5 were established from the cosine sub-bundle test series summarized in Table 3.1. They were developed for the XL-S96 correlation as described in Reference 1. The additive constants developed for the XL-S96 correlation were retained for ABBD1.0. This approach is justified by the correlation evaluation in Section 5 which demonstrates that the additive constants developed for XL-S96, in conjunction with the optimized ABBD1.0 correlation parameters, provide a good fit to the expanded SVEA-96 data base containing cosine, top-peaked and bottom-peaked axial power shapes.

It should be noted that the principles used to develop the additive constants for XL-S96 are same as those used to establish the additive constants for ABBD2.0. Detailed descriptions of the development of the ABBD2.0 additive constants and the associated uncertainties were presented in the responses to Request Numbers 13 and 34 in Reference 6 .

2. **[Proprietary Information Deleted].**
3. **[Proprietary Information Deleted].**

#### 4.5 Assembly R-Factor - Treatment of Sub-bundle Power Mismatch

**[Proprietary Information Deleted]:**

1. The methodology used to establish the mismatch factor for ABBD1.0 is the same as that used for ABBD2.0 in Reference 5. The actual mismatch factor established by this methodology is specific to the ABBD1.0 correlation and reflects the actual SVEA-96 characteristics.

2. The radial configuration of the sub-bundles and integral water cross channel are identical for the SVEA-96 and SVEA-96+ assemblies. The minor differences between the SVEA-96 and SVEA-96+ designs are only an additional spacer in the SVEA-96+ design and a minor modification in the spacer design. Expansion of the sub-bundle R-factor to the full assembly involves calculations of the radial flow redistribution between the sub-bundles. The relatively minor impact of the differences in spacer arrangement and design on the radial flow redistribution is captured by applying the methodology separately for both assembly designs.

**[Proprietary Information Deleted].**

The quantity, R, is the R-factor which is input to the ABBD1.0 correlation for full assembly applications.

**FIGURES 4.1 THROUGH 4.6**  
**[PROPRIETARY INFORMATION DELETED]**

## 5. CORRELATION EVALUATION

The functional form of the ABBD1.0 dryout correlation has been developed to correlate the critical power test data in the critical quality-boiling length plane.

The ABBD1.0 CPR correlation data base is composed of a total of **[Proprietary Information Deleted]** steady state critical power measurements. Evaluation of the ABBD1.0 CPR correlation relative to the steady state data base is contained in this section. In addition, Section 6 contains the evaluation of the ABBD1.0 CPR correlation relative to transient critical power measurements.

The steady state CPR data base is composed of **[Proprietary Information Deleted]** points measured with a full scale 24-rod sub-bundle. This critical power data base was divided into two data sets. The **[Proprietary Information Deleted]** evaluation data set represented 80% of the data base and was used in the correlation derivation. The **[Proprietary Information Deleted]** validation data set represents 20% of the data base and was used for validation of the ABBD1.0 CPR correlation. The number of data points and local power distributions for the evaluation and validation data sets are summarized in Table 5.1 and 5.2, respectively.

The 24-rod SVEA-96 data base obtained with a cosine axial power distribution is discussed in Reference 1. The results of the measurements obtained with the cosine axial power shape are shown in Appendix A of Reference 1, and the test bundle local power distributions used to generate that data base are shown in Figure 3.1 of Reference 1. The 24-rod SVEA-96 data base obtained with the bottom-peaked axial power distribution and test bundle local power distributions used to generate that data base are shown in Appendix B. The 24-rod SVEA-96 data base with the top-peaked axial power distribution and the test bundle local power distributions used to generate that data base are shown in Appendix C.

### 5.1 ABBD1.0 Performance Relative to the SVEA-96 Data Base

Table 5.3 shows mean prediction errors, standard deviations, numbers of data points, and 95/95 tolerance limits for the ABBD1.0 CPR correlation relative to the entire 24-rod SVEA-96 data base as well as relative to subsets of that data base.

The prediction error,  $\varepsilon$ , is given by:

$$\varepsilon = \left[ \frac{\text{predicted power}}{\text{measured power}} - 1 \right] \times 100 \quad \text{Equation 5-1}$$

As shown in Table 5.3, the mean prediction error and standard deviation over the entire SVEA-96 data base is **[Proprietary Information Deleted]**. The mean prediction error and standard deviation over the validation data set is **[Proprietary Information Deleted]**. Since the validation data set was selected in a systematic, unbiased manner over the entire data base, the fact that the statistics in Table 5.3 **[Proprietary Information Deleted]**.

A useful graphical validation technique for a calculated function is to plot the function versus the measured values. Figure 5.1 is a comparison of the critical powers predicted with the ABBD1.0 correlation as a function of the measured

critical powers for all **[Proprietary Information Deleted]** data points used to develop and validate the correlation. The solid lines in Figure 5.1 represent variations from the correlation prediction of  $\pm 5\%$ . The designations "C", "B", and "T" refer to data obtained with chopped cosine, bottom-peaked, and top-peaked axial power distributions, respectively. As shown in Figure 5.1, the ABBD1.0 correlation shows good agreement with the measured data and does not show a bias as a function of critical power. Table 5.4 provides the number and percentage of predictions exceeding the 5% boundary.

Another standard graphical validation technique is to plot the prediction error,  $\varepsilon$ , versus parameters to which the function is sensitive. An ideal prediction is characterized by  $\varepsilon = 0.0$ . Accordingly, the prediction error is plotted as a function of **[Proprietary Information Deleted]** in Figures 5.2 through 5.8. The prediction error,  $\varepsilon$ , is defined by Equation 5-1.

Figure 5.2 is a plot of the prediction error for the ABBD1.0 correlation relative to the entire **[Proprietary Information Deleted]**.

Figure 5.4 is a plot of the prediction error for the ABBD1.0 correlation relative to the entire **[Proprietary Information Deleted]**.

Figure 5.5 is a plot of the prediction error for the ABBD1.0 correlation relative to the **[Proprietary Information Deleted]**.

Figures 5.6 and 5.7 are plots of the prediction error for the ABBD1.0 correlation relative to the **[Proprietary Information Deleted]**.

Figure 5.8 is a plot of the prediction error for the ABBD1.0 correlation relative to the **[Proprietary Information Deleted]**.

In Summary, Figures 5.2 through 5.8 demonstrate that the ABBD1.0 correlation provides a good fit to the test data with no systematic biases which would limit the validity of the correlation to predict the bundle critical power performance in design and licensing applications.

Figure 5.9 is a frequency distribution of the prediction error for the SVEA-96 data base. **[Proprietary Information Deleted]**.

Figure 5.10 shows critical power dependence on axial power shape and mass flux predicted by ABBD1.0. Note that the intent of Figure 5.10 is to show the trends for various axial power shapes. A nominal condition is assumed for these correlation predictions. There are no measured data at these precise conditions for direct comparison. As shown in Figure 5.10, **[Proprietary Information Deleted]**.

Similarly, Figure 5.11 shows the ABBD1.0 critical power dependence on inlet subcooling for several different mass flux values. As shown in Figure 5.11, **[Proprietary Information Deleted]**.

Table 5.5 shows the mean error, standard deviation, number of data points and 95/95 tolerance limits **[Proprietary Information Deleted]**.

Figure 5.12 to Figure 5.14 present essentially the same information as Figure 5.2. Instead of the prediction error, the ratio of the predicted critical power to the measured critical power is plotted as a function of mass flux for each of the axial power profiles. Table 5.6 provides the mean, standard deviations and number of data points for the various mass flux ranges.

Additional plots of the prediction error as a function of mass flux, pressure, and inlet subcooling at selected regions covering the fringe area of operation are presented in Figures 5.15 through 5.32. As can be seen from these figures, with the exception of Figure 5.17, there are no significant trends or biases. These figures demonstrate that ABBD1.0 CPR correlation is applicable in the fringe area of operation (with sufficient data points) as well as near the nominal condition (with a majority of data points). Figure 5.17 shows a small bias. At high pressure (85 bar) and high mass flux ( $> 1400 \text{ kg/m}^2\text{-s}$ ), the prediction errors become more negative. However, this bias does not have any significant impact on reactor application since a negative error implies a more conservative (e.g., lower) lower prediction of critical power.

In summary, the following conclusions can be drawn from comparison of the ABBD1.0 correlation predictions with the 24-rod SVEA-96 data base:

1. All trends in the critical power data base discussed in Section 3 are adequately captured with the ABBD1.0 CPR correlation. Furthermore, predicted critical power trends with **[Proprietary Information Deleted]** are consistent with previous dryout testing of earlier assembly designs.
2. The quality of the predictions of the ABBD1.0 CPR correlation does not show any evidence **[Proprietary Information Deleted]**.
3. Therefore, it is concluded that the ABBD1.0 CPR correlation provides a satisfactory fit to the data to justify its use for design and licensing applications. A normal uncertainty distribution with a mean error of **[Proprietary Information Deleted]** provides a good characterization of the prediction error distribution for the SVEA-96 data base.

## 5.2

### Correlation Uncertainty and Range of the Correlation

Based on the evaluations in Section 5.1, it is concluded that the best estimate of the ABBD1.0 CPR correlation mean prediction error and standard deviation in the mean prediction error should be based on the **[Proprietary Information Deleted]**. Therefore, from Table 5.3, a mean prediction error and standard deviation of **[Proprietary Information Deleted]** will be used for design and licensing applications. A detailed description of the treatment of the correlation uncertainty in a design and licensing application is provided in Reference 6 (See ABB Response to NRC Request Number 13).

The range over which the ABBD1.0 CPR correlation is valid is shown in Table 5.7. This range is based on the **[Proprietary Information Deleted]**.

**TABLES 5.1 THROUGH 5.7**  
**[PROPRIETARY INFORMATION DELETED]**

**FIGURES 5.1 THROUGH 5.32**

**[PROPRIETARY INFORMATION DELETED]**

## 6. CONFIRMATION FOR TRANSIENT APPLICATION

### 6.1 Introduction

One specified acceptable fuel design limit (SAFDL) is that no more than 0.1% of the fuel rods in the core experience boiling transition under normal operation and anticipated operational occurrences. This requirement is equivalent to maintaining a certain transient Critical Power Ratio (CPR).

Transient CPR predictions involve evaluation of the flow, enthalpy, and pressure in the fuel assembly at each axial node as a function of time during the transient. A transient systems analysis code is used to calculate the transient fluid parameters. These parameters are then used with the steady-state CPR correlation for an assembly to evaluate transient CPR. One transient systems analysis code used by ABB for CPR predictions is the BISON-SLAVE channel model of the BISON transient analysis code (Reference 2). In licensing analysis applications the plant Operating Limit Minimum Critical Power Ratio (OLMCPR) is determined based, in part, on calculations with a transient systems analysis code. The OLMCPR is established to ensure that the Safety Limit Minimum Critical Power Ratio (SLMCPR) is not violated.

Two transient test programs are available to confirm that the ABBD1.0 CPR correlation in conjunction with the BISON-SLAVE channel model provides conservative  $\Delta$ CPR predictions during transient applications. The first program is the qualification of the ABBD2.0 CPR correlation for transient applications described in Reference 5. [Proprietary Information Deleted] flow reduction transient tests and [Proprietary Information Deleted] power increase transient tests were used to confirm that the ABBD2.0 CPR correlation for SVEA-96+ fuel in conjunction with the BISON-SLAVE channel model provide conservative CPR results during transient applications. Specifically, it was demonstrated in Reference 5 that transient CPR results were conservatively predicted in over 98% of the cases. The three non-conservative results were only marginally non-conservative and were well within the measurement uncertainty. These results for ABBD2.0 in Reference 5 are considered to provide confirmation that the ABBD1.0 CPR correlation in conjunction with the BISON-SLAVE code will also predict conservative results. Both correlations use [Proprietary Information Deleted]. Therefore, the program described in Reference 5 to qualify the ABBD2.0 CPR correlation for transient application for the SVEA-96+ assembly is considered to provide confirmation that the ABBD1.0 CPR correlation with the BISON-SLAVE code will predict conservative CPR results during a transient involving the SVEA-96 assembly.

The second test program confirming that the ABBD1.0 CPR correlation in conjunction with the BISON-SLAVE channel model provides conservative transient  $\Delta$ CPR predictions is described in Section 7 of Reference 1. This program validated the application of the XL-S96 CPR correlation in conjunction with the BISON-SLAVE code for transient applications using the same process as used for the ABBD2.0 CPR correlation in Reference 5. Use of these SVEA-96 tests described in Section 7 of Reference 1 to confirm that the ABBD1.0 CPR correlation in conjunction with the BISON-SLAVE code provides an additional confirmation of the conservative treatment of CPR during transient application. This additional verification is described in this section.

The methodology for confirming that the application of the ABBD1.0 correlation in transient calculations will provide conservative predictions of  $\Delta\text{CPR}$  is summarized in this section. Specifically, the process for qualifying implementation of the ABBD1.0 correlation in transient codes is described. Then, the transient experiments performed in the FRIGG test loop and described in Section 7 of Reference 1 are summarized. Finally, the ABBD1.0 correlation validation in the BISON-SLAVE transient code is presented. The methodology used to confirm the adequacy of the ABBD1.0 correlation for transient applications described in this section is the same as the illustration for ABBD2.0 described in Reference 5.

## 6.2 Transient Implementation Validation Methodology

The two objectives of the transient systems analysis code implementation validation are to:

1. Confirm proper implementation of the steady state CPR correlation in the transient code.
2. Confirm the capability of the steady-state CPR correlation implemented in the transient code to calculate dryout during transients with adequate accuracy to provide conservative predictions of  $\Delta\text{CPR}$ .

Transient code implementation of the ABBD1.0 CPR correlation is validated for each code application by **[Proprietary Information Deleted]**.

## 6.3 Transient Dryout Experiments

The transient tests used to validate the XL-S96 correlation were described in detail in Section 7 of Reference 1. The use of these tests to validate the ABBD1.0 correlation for transient applications is described in this section.

### 6.3.1 FRIGG Loop

The transient tests were performed with the same test facility used in the steady-state experiments described in Section 2 of Reference 1.

As discussed in Reference 1, flow reduction transients with a SVEA-96 test assembly were simulated in the FRIGG loop transient tests. The FRIGG loop transients cases **[Proprietary Information Deleted]**. These flow reduction transients were performed by varying the speed of the recirculation pump positioned in the main circulation loop as well as the heater rod power.

Dynamic heater rod thermocouple responses are recorded during the transient tests. In addition, transient test system response data are recorded in order to provide time-dependent boundary conditions for the transient system code calculations. The test section inlet coolant flow, pressure, temperature and the total power production are recorded.

### 6.3.2 Test Section

The test section used for the transient tests is identical to the test section (SF24A) used for steady state tests. The local power distribution used in the transient tests is shown in Figure 6.1.

### 6.3.3 Transient Tests Description

Flow reduction event simulations were used for the XL-S96 CPR correlation validation for transient applications in Reference 1. The same data discussed in Reference 1 were used to validate the use of ABBD1.0 for transient applications. The flow reduction transient is characterized as follows:

1. The mass flow to the test section was reduced from about 3 kg/s to 1 kg/s (6.6 lb/s to 2.2 lb/s) in about 4 seconds.
2. The reduction in flow rate was followed by a reduction of the power supplied to the heater rods. The heater rod power reduction was initiated between 0.5 to 2.5 seconds after the flow reduction was initiated.

The general transient behavior is shown schematically in Figure 6.2.

### 6.3.4 Dryout Threshold Temperature

The dryout threshold temperature is the temperature increase during the transient which is assumed to indicate dryout (e.g., CPR equals 1.0). As described in Reference 1, a dryout threshold temperature [Proprietary Information Deleted].

### 6.3.5 Transient Data

Five transient tests were performed in Reference 1 and used for the transient CPR performance evaluation. All five cases have the same general transient behavior as shown in Figure 6.2.

The initial test section conditions (power and mass flow) and the delay between the start of flow coastdown and the start of power reduction were varied. These data, as well as the power and mass flow conditions in the final state of the transient, are summarized in Table 6.1. The pressure was maintained at about 7 MPa (1015 psia), and the inlet subcooling was maintained at about 10 °C (18 °F) in all the 5 cases.

Boundary conditions for these five flow reduction tests are shown in Figures 6.3 through 6.7. Figures 6.3 through 6.7 show heater rod power level, inlet coolant flow, test section inlet pressure, and inlet coolant temperature applied to the test section as a function of time.

Table 6.2 summarizes the lead thermocouple readings. Based on the dryout threshold temperature of [Proprietary Information Deleted] dryout was detected in cases 1435, 1437 and 1440. No indication of dryout was detected during test numbers 1394 and 1395.

## 6.4 Implementation Validation for BISON Code

The BISON-SLAVE channel model of the time domain reactor dynamics code BISON (Reference 2) will be used in conjunction with the ABBD1.0 CPR correlation to predict transient CPR behavior for reload fuel licensing analysis applications and other operational transient simulations. The BISON-SLAVE simulations presented in this section are an illustration of the methodology described in Section 6.2 for confirming that the use of a CPR correlation based on steady-state data is acceptable for transient application.

An overview of the BISON code and test section model is described below. Then, the transient test simulation results for the flow reduction tests are presented. It will be shown that the BISON-SLAVE predictions of transient dryout are conservative for all tests confirming the conservative calculation of transient CPR performance.

#### 6.4.1 BISON Code

BISON is a time domain BWR dynamics code used for analyzing operational and safety related transients. The code simulates the hydraulics of the entire primary core coolant loop including the recirculation pumps. A two-group diffusion theory model describes the axial distributions of neutron flux and power in the reactor core. Heat conduction in the fuel is solved in the radial direction at each axial segment. The influence from external systems such as the turbine, control systems, scram signals, and relief valves can also be simulated in BISON.

A BISON-SLAVE version of the code is used for simulation of a single bundle in the core by utilizing boundary conditions from a previous BISON calculation for the entire reactor. It can also be used in a stand-alone mode to study heated bundles in loop experiments. External boundary conditions in the form of inlet mass flow and temperature, inlet pressure, and assembly power are supplied as input to the code. This option was used in the present evaluation to calculate the transient critical power ratio (CPR) for the experiments performed.

The ABBD1.0 CPR correlation is incorporated in the BISON-SLAVE code. Instantaneous fluid properties [Proprietary Information Deleted] are used in evaluating the CPR correlation under transient conditions.

#### 6.4.2 BISON Model

[Proprietary Information Deleted] are modeled in the BISON simulations of the tests. The heated part of the test section is simulated with the BISON-SLAVE channel model. The heater rod is modeled with the same radial nodal divisions typically used in plant calculations. The radial representation and material compositions of the heater rod are shown in Figure 6.8.

The experimental conditions described in the previous sections were used as input to the BISON-SLAVE model. [Proprietary Information Deleted] The power is provided as a boundary condition for the heater rods in the test assembly. The axial and local rod radial power distributions are [Proprietary Information Deleted]. The outlet pressure and inlet flow and subcooling are also provided as boundary conditions.

The R-factors for the local power distributions (Figure 6.1) used in the flow reduction tests were determined [Proprietary Information Deleted].

#### 6.4.3 BISON Test Simulation Results

All five tests were simulated with the BISON-SLAVE code. The calculated transient CPR results are shown in Table 6.3. [Proprietary Information Deleted].

The predicted times to dryout [Proprietary Information Deleted] are compared with the measured times to dryout [Proprietary Information Deleted] in Table 6.4. [Proprietary Information Deleted].

## 6.5 Summary

The systematic ABB methodology used to confirm the conservative application of a CPR correlation for transient CPR code applications is illustrated in this section for the ABBD1.0 CPR correlation. The results in Reference 5 and the comparisons of BISON-SLAVE code predictions with SVEA-96 sub-bundle test results in this section demonstrate that the ABBD1.0 CPR correlation is capable of providing conservative estimates of the onset of dryout during fast transients.

**TABLES 6.1 THROUGH 6.4**

**[PROPRIETARY INFORMATION DELETED]**

**FIGURES 6.1 THROUGH 6.8**  
**[PROPRIETARY INFORMATION DELETED]**

## 7. CONCLUSIONS

The critical power measurements described in this report provide an accurate simulation of the SVEA-96 fuel assembly. A total of **[Proprietary Information Deleted]** 24-rod sub-bundle data points covering the entire range expected during reactor operation were obtained. The ABBD1.0 critical power ratio correlation was developed to correlate this critical power data. The correlation was developed to provide best estimate predictions of critical power for a SVEA-96 fuel assembly. The mean prediction error and standard deviation over the entire range of validity are **[Proprietary Information Deleted]**.

Based on the critical power data for SVEA-96 and the evaluations of the data presented in this report, the following conclusions can be drawn:

1. Sufficient data have been obtained to justify the use of the correlation over the following ranges for design and licensing applications:

### TABLE 7.1 [PROPRIETARY INFORMATION DELETED]

These ranges cover the operating conditions expected during U.S. BWR steady-state, transient, or accident conditions over which CPR calculations are expected to be required.

2. The correlation provides a best estimate of the bundle Critical Power Ratio over the range of validity and, is, therefore, acceptable for evaluations of Critical Power Ratios for design and licensing purposes over this range.
3. The mean prediction error and standard deviation to be utilized for the correlation for design and licensing applications is **[Proprietary Information Deleted]** are appropriate for computing core Safety Limit Minimum Critical Power Ratios (SLMCPR).
4. The correlation has been demonstrated to be capable of providing conservative estimates of the onset of dryout during fast transients. The capability of the correlation to provide conservative estimates of the onset of dryout during fast transients is demonstrated for each transient system code application. An illustration of the ABB methodology for confirming the capability of the correlation to conservatively treat transient applications is provided for the BISON-SLAVE code documented in Reference 2. It is demonstrated in this illustration that the correlation, in conjunction with the BISON-SLAVE code, is acceptable for the calculation of changes in CPR during transient events for design and licensing applications.

**8. REFERENCES**

1. "SVEA-96 Critical Power Experiments on a Full Scale 24-Rod Sub-Bundle", ABB Report UR-89-210-P-A, October 1993.
2. "BISON - A One Dimensional Dynamic Analysis Code for Boiling Water Reactors", ABB Report RPA 90-90-P-A, December 1991.  
  
"BISON - One Dimensional Dynamic Analysis Code for Boiling Water Reactors: Supplement 1 to Code Description and Qualification", ABB Report CENPD-292-P-A, July 1996.
3. "General Electric BWR Thermal Analysis Basis (GETAB): Data, Correlation and Design Application", NEDO-10958, November 1973.
4. "CONDOR: A Thermal-Hydraulic Performance Code for Boiling Water Reactors", ABB Report BR 91-255-P-A, Rev. 1, (Proprietary), BR 91-262-NP-A (Non-proprietary), May 1991.
5. "10x10 SVEA Fuel Critical Power Experiments and CPR Correlations: SVEA-96+", ABB Report CENPD-389-P, June 1998.
6. "Response to Request for Additional Information Regarding CENPD-389-P", Letter, I. C. Rickard (ABB) to USNRC Document Control Desk, LD-99-019, April 9, 1999.
7. "Acceptance for Reference of Licensing Topical Report CENPD-389-P, 10x10 SVEA Fuel Critical Power Experiments and CPR Correlations: SVEA-96+", Letter, C. A. Carpenter (NRC) to I. C. Rickard (ABB), May 8, 1999.

**APPENDIX A****SVEA-96 ASSEMBLY DESCRIPTION**

The SVEA96 assembly is shown in Figures A-1 and A-2. The fuel assembly consists of 96 fuel rods arranged in four subbundles, each with a 5x5-1 lattice. Each subbundle is a separate unit with top and bottom tie plates. The fuel rods are supported laterally by six spacers, distributed uniformly along the bundle. The channel has a cruciform internal structure (watercross) with a square center channel and cross wings with gaps for non-boiling water during normal operation.

**Figure A-1**

**[Proprietary Information Deleted]**

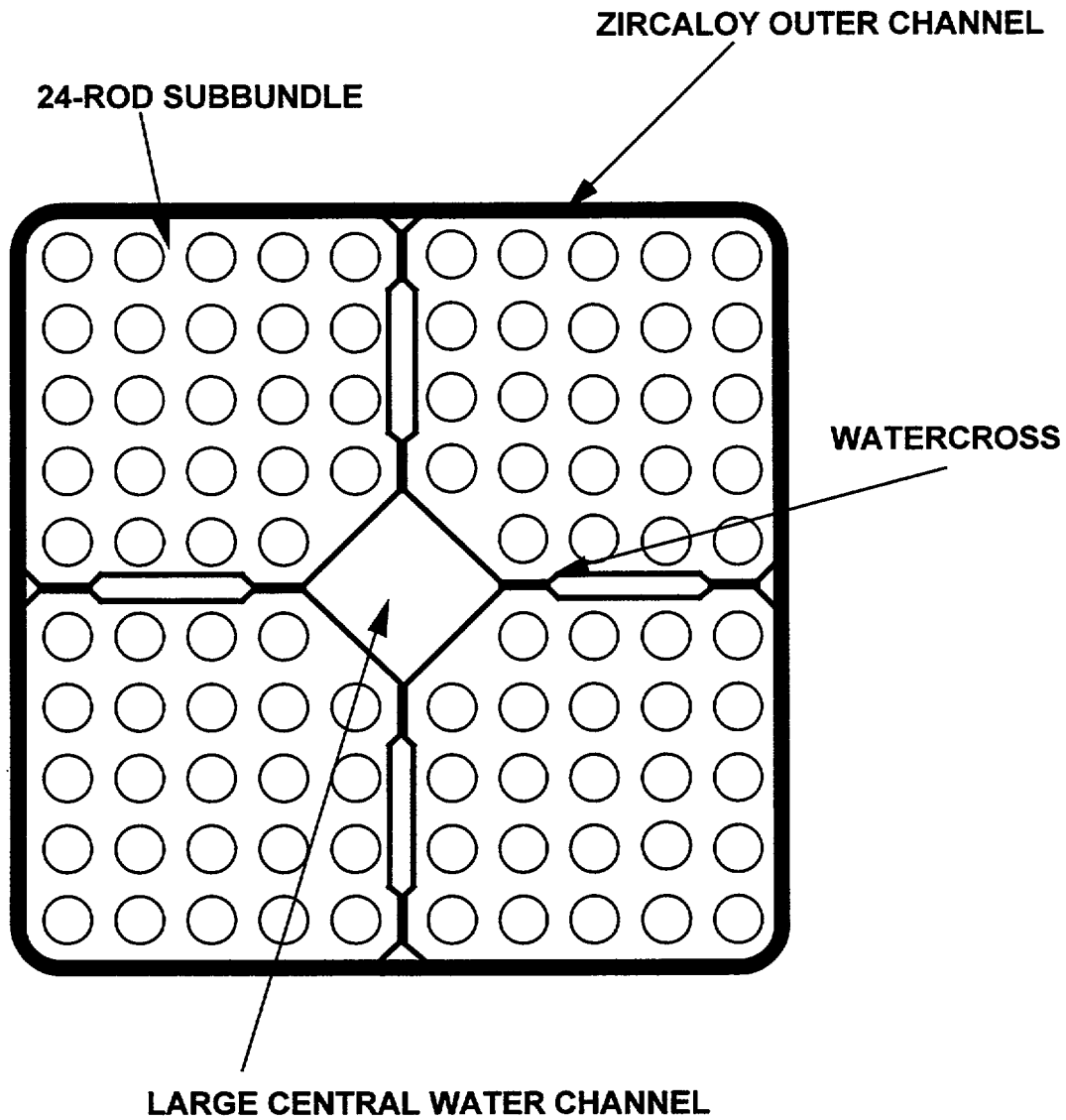


Figure A-2 SVEA96 Fuel Assembly Cross Section

**APPENDIX B****SVEA 96 STEADY STATE CRITICAL POWER TEST DATA  
(BOTTOM-PEAKED AXIAL POWER SHAPE)**

ID	The identity of the measurement point
P	The system pressure (bar)
T <sub>sub</sub>	Subcooling temperature (K)
Flow	Mass flow (kg/s)
Power	Bundle power at dryout (kW)
Y/I	The ratio between the average local power for the 15 peripheral rods and the average local power for the 9 central rods
Rod	The rod(s) and its/their thermocouples indicating dryout (refer to Figure 2.3 for rod location and Figure 2.6 for thermocouple location, e.g. 107.14 means rod 7 in Figure 2.3 and T/C level 14 in Figure 2.6)

The local power distribution map at about 3 kg/s flow is printed on each page together with a critical power versus mass flow plot with all separate dryout points. When the local power distribution map is not printed, it has been shown for a previous test series.

It must, however, be noted that the local power distribution may differ slightly for different points intended to have the same nominal distribution (e.g. AA4, AA5, etc.). The actual measured local power distributions were used for all points in the correlation development and validation process.

**TABLES AND FIGURES****[PROPRIETARY INFORMATION DELETED]**

**APPENDIX C****SVEA 96 STEADY STATE CRITICAL POWER TEST DATA  
(TOP-PEAKED AXIAL POWER SHAPE)**

ID	The identity of the measurement point
P	The system pressure (bar)
T <sub>sub</sub>	Subcooling temperature (K)
Flow	Mass flow (kg/s)
Power	Bundle power at dryout (kW)
Y/I	The ratio between the average local power for the 15 peripheral rods and the average local power for the 9 central rods
Rod	The rod(s) and its/their thermocouples indicating dryout (refer to Figure 2.3 for rod location and Figure 2.7 for thermocouple location, e.g. 107.01 means rod 7 in Figure 2.3 and T/C level 1 in Figure 2.7)

The local power distribution map at about 3 kg/s flow is printed on each page together with a critical power versus mass flow plot with all separate dryout points. When the local power distribution map is not printed, it has been shown for a previous test series.

It must, however, be noted that the local power distribution may differ slightly for different points intended to have the same nominal distribution (e.g. AA4, AA5, etc.). The actual measured local power distributions were used for all points in the correlation development and validation process.

**TABLES AND FIGURES****[PROPRIETARY INFORMATION DELETED]**

# **ABB Combustion Engineering Nuclear Power, Inc.**

ABB Combustion Engineering Nuclear Power, Inc.  
2000 Day Hill Road  
Post Office Box 500  
Windsor, Connecticut 06095-0500